

Finite element simulation of three-dimensional free-surface flow problems

M.A. Walkley^{1,*}, P.H. Gaskell², P.K. Jimack¹,
M.A. Kelmanson³ and J.L. Summers²

¹ School of Computing,

² School of Mechanical Engineering,

³ Department of Applied Mathematics,

University of Leeds, Leeds, LS2 9JT, UK

* Corresponding author: markw@comp.leeds.ac.uk,
Tel.: +44(0)113 3435684, Fax.: +44(0)113 3435468

Running head: *Finite element simulation of
three-dimensional free-surface flow problems*

February 25, 2004

Abstract

An adaptive finite element algorithm is described for the stable solution of three-dimensional free-surface-flow problems based primarily on the use of node movement. The algorithm also includes a discrete remeshing procedure which enhances its accuracy and robustness. The spatial discretisation allows an isoparametric piecewise-quadratic approximation of the domain geometry for accurate resolution of the curved free surface. The technique is illustrated through an implementation for surface-tension-dominated viscous flows modelled in terms of the Stokes equations with suitable boundary conditions on the deforming free surface. Two three-dimensional test problems are used to demonstrate the performance of the method: the extension of a liquid bridge and the evolution of a fluid droplet.

Keywords: Finite element method; Free-surface flow; Moving grids

1 INTRODUCTION

Free-surface flow problems occur in a wide variety of scientific and engineering applications. Examples include phase-change problems [13, 27], coating flows [8, 25], the spreading of viscous fluids [14, 17] and the motion of drops or bubbles [3, 32]. The primary interest of this paper is the development of a numerical technique for the solution of time-dependent free-surface flows in three dimensions, which represents one of the most important practical computational challenges for this class of problem. The requirement for time-dependence is apparent in almost all applications since understanding the evolution and stability of free surfaces provides one of the major incentives for their mathematical and computational study. Furthermore, fully three-dimensional simulations are required in order to capture all of the physically important features of most free-surface flows. For example, in [21] a robust two-dimensional scheme is used to model the gravity-driven shedding of a curtain of fluid from a long rotating cylinder, however this work necessarily ignores both end effects and time-dependent perturbations in the flow parallel with the axis of the cylinder.

In recent years there has been a significant amount of work relating to the computational study of time-dependent free-surface flows. Simplifying assumptions can often be made, such as restriction to two dimensions (e.g. [15, 20, 35]), or the use of a lubrication approximation based upon assumptions of a relatively thin liquid film with negligible flow variation across the film (e.g. [6, 7, 23, 29]). Fully three-dimensional studies have also been undertaken based upon a variety of computational techniques. These include the use of finite-difference-based marker-and-cell methods [16, 34], volume-of-fluid methods [5, 10], level-set methods [19, 30], and techniques based upon the finite element method using moving grids [1, 4, 27, 31, 38]. The last approach is the one pursued in this paper.

Each of the popular classes of method that may be used to tackle three-dimensional moving boundary problems has its relative strengths and weaknesses; we do not begin to attempt to analyse these fully here but instead refer the reader to, for example, [26]. Typically, however, moving-grid finite-element approaches are not well suited to problems for which the topology of the free surface changes discontinuously with time, as occurs in, for example, the break-up of a single droplet into two, or the coalescence of two droplets into one. In these situations special intervention is needed, requiring both detection and effective resolution when topology changes occur. The level-set and the volume-of-fluid methods deal with these situa-

tions in a far more robust manner. The level-set method does so at the expense of introducing an additional dependent variable throughout the entire problem domain. The volume-of-fluid approach, whilst also being robust, tends to suffer from low accuracy due to the piecewise constant representation of the interface.

When the topological index of the moving surface does not change during flow evolution, moving-grid finite element approaches have the twofold advantage of (a) requiring computation within only the region occupied by the fluid of interest, and (b) the ability to represent the free surface to a high degree of accuracy. Typically, as in this research, work using moving grids has tended to be based upon the arbitrary Lagrangian-Eulerian (ALE) approach, [4, 20, 38], whereby the free surface may evolve with the fluid but the interior grid evolves according to geometric constraints, rather than following the physical flow (as in the Lagrangian approach of [18, 24]).

The numerical technique described in this paper is a generalisation of both the two-dimensional algorithm introduced in [20] and the three-dimensional technique of [4]. The principal extensions that are presently introduced are: to provide a three-dimensional incompressible free-surface flow solver based upon the use of implicitly stable elements (the so-called Taylor-Hood element [9]); to represent the three-dimensional free surface using piecewise-quadratic patches for optimal accuracy with the chosen elements (this is of particular significance when surface tension effects are dominant); to implement the three-dimensional moving-mesh algorithm in conjunction with a discrete-mesh regeneration procedure (to allow for larger geometry changes to occur than is otherwise possible), and; to apply the scheme to a wide range of surface-tension-dominated viscous-flow problems.

In Section 2 the mathematical formulation of the underlying problem is briefly outlined, along with a short description of the most significant assumptions that are made. Section 3 then provides details of the numerical scheme that is proposed. A number of important issues are described including the underlying discretisation, the mesh-movement algorithm (both on the free surface and throughout the rest of the domain), the use of a curved boundary representation (and the evaluation of surface tangents and normals), the solution of the algebraic systems of equations that follow the discretisation, the issues associated with contact lines, and the implementation of the boundary conditions at the moving surface. Section 4 illustrates the performance of the method by testing it on a range of examples. This motivates the

requirement for a discrete remeshing step within the algorithm, the implementation of which is also discussed. The improved robustness obtained through a combination of continuous mesh movement and discrete mesh regeneration is then demonstrated. The paper concludes with a brief discussion of the strengths and current limitations of the work, as well as some suggestions for further study.

2 MATHEMATICAL MODEL

The focus is three-dimensional incompressible flows governed by a non-dimensionalised form of the Navier-Stokes equations. Starting with the standard dimensional form for momentum conservation (with velocity \mathbf{u} , pressure p , density ρ , dynamic viscosity μ and gravity g acting in direction of unit vector \mathbf{f}),

$$\rho \left(\frac{\partial \mathbf{u}}{\partial t} + (\mathbf{u} \cdot \nabla) \mathbf{u} \right) = -\nabla p + \mu \nabla \cdot (\nabla \mathbf{u} + (\nabla \mathbf{u})^T) + \rho g \mathbf{f}, \quad (1)$$

it is possible to non-dimensionalise with respect to length and velocity scales L and U and time and pressure scales L/U and $\mu U/L$ respectively. This leads to the system

$$\frac{\rho U L}{\mu} \left(\frac{\partial \mathbf{u}}{\partial t} + (\mathbf{u} \cdot \nabla) \mathbf{u} \right) = -\nabla p + \nabla \cdot (\nabla \mathbf{u} + (\nabla \mathbf{u})^T) + \frac{\rho g L^2}{\mu U} \mathbf{f}, \quad (2)$$

which may be expressed as

$$Re \left(\frac{\partial \mathbf{u}}{\partial t} + (\mathbf{u} \cdot \nabla) \mathbf{u} \right) = \nabla \cdot \boldsymbol{\sigma} + St \mathbf{f}, \quad (3)$$

where the non-dimensional Reynolds number Re and Stokes number St are given by

$$Re = \frac{\rho U L}{\mu}, \quad St = \frac{\rho g L^2}{\mu U}, \quad (4)$$

and $\boldsymbol{\sigma}$ (the stress tensor) is

$$\boldsymbol{\sigma} = -p \mathbf{I} + \nabla \mathbf{u} + \nabla \mathbf{u}^T. \quad (5)$$

One further non-dimensional parameter of relevance to this problem (see the stress boundary condition at the free surface, (9) below) is the capillary number,

$$Ca = \frac{\mu U}{\tau}. \quad (6)$$

Here τ is the surface tension, which is assumed to be constant over the entire free surface.

For the purposes of this work we concentrate on viscous flows that are driven mainly by surface-tension effects at the free surface and external body forces such as gravity. Hence throughout the paper we consider the slow-flow case $Re \ll 1$, for which the left-hand side term in (3) may be neglected. When combined with mass conservation for an incompressible fluid the governing system simplifies to

$$\mathbf{0} = \nabla \cdot \boldsymbol{\sigma} + St\mathbf{f}, \quad (7)$$

$$0 = \nabla \cdot \mathbf{u}, \quad (8)$$

in a fluid domain Ω with boundary Γ . A no-slip boundary condition is applied at solid boundaries, and at the free surface the normal stress condition

$$-\boldsymbol{\sigma} \cdot \mathbf{n} = p_{ext}\mathbf{n} - \frac{1}{Ca}(\nabla_s \cdot \mathbf{n})\mathbf{n}, \quad (9)$$

is applied, where \mathbf{n} is the outward unit normal and ∇_s represents the surface gradient operator given by $\nabla_s = (\mathbf{I} - \mathbf{nn}) \cdot \nabla$. For the purposes of this work it is assumed (without loss of generality) that the external pressure p_{ext} is zero. In addition, at the free surface, a kinematic boundary condition

$$\mathbf{n} \cdot (\mathbf{u} - \dot{\mathbf{x}}) = 0, \quad (10)$$

also applies, where a dot superscript refers to differentiation with respect to non-dimensionalised time t . This time dependent boundary condition describes the evolution of the free-surface geometry, driven by the velocity field.

3 NUMERICAL SCHEME

An ALE solution algorithm is employed to solve this problem. The geometry and flow field evolve in time due to the motion of the free surface and hence in general the problem is both time-dependent and nonlinear. However, since the only time-dependent and nonlinear terms are contained in the kinematic boundary condition (10), the interior flow and surface evolution may be decoupled in the following way. For each single timestep:

1. solve the (steady, linear) Stokes equations (7)-(8) on the current geometry to find \mathbf{u} and p ;

2. update the free-surface position with the (time-dependent, nonlinear) kinematic boundary condition (10);
3. update the interior mesh.

3.1 Solution of the Stokes Equations

The Stokes equations (7)-(8) are discretised in space with an isoparametric tetrahedral Taylor-Hood finite element method [9]. This choice is *a priori* LBB stable and has the additional advantage of including an isoparametric, quadratic representation of the free surface. This allows more accurate modelling of the surface curvature, and hence the free-surface stress boundary condition (9), than has been previously used [4, 38] in three-dimensional models for this class of problem.

Defining ϕ_i and ψ_j as the respective quadratic and linear basis functions from the Taylor-Hood space, the finite element approximation is developed by multiplying each of the components, α say, of the momentum equation (7) with ϕ_i and multiplying (8) with ψ_j and integrating over the spatial domain Ω . This yields

$$0 = \int_{\Omega} \phi_i (\nabla \cdot \boldsymbol{\sigma} + St \mathbf{f})_{\alpha} d\Omega \quad \alpha = 1, 2, 3; \quad i = 1, \dots, N_v, \quad (11)$$

$$0 = \int_{\Omega} \psi_j (\nabla \cdot \mathbf{u}) d\Omega \quad j = 1, \dots, N_p, \quad (12)$$

where N_v and N_p are the number of non-Dirichlet velocity and pressure nodes respectively. The momentum equations (11) is integrated by parts to give

$$\begin{aligned} \int_{\Omega} (-\nabla \phi_i \cdot \boldsymbol{\sigma} + St \phi_i \mathbf{f})_{\alpha} d\Omega &= - \int_{\Gamma} (\phi_i \boldsymbol{\sigma} \cdot \mathbf{n})_{\alpha} d\Gamma, \\ &= - \int_{\Gamma_f} \phi_i \frac{1}{Ca} (\nabla_s \cdot \mathbf{n}) n_{\alpha} d\Gamma, \end{aligned} \quad (13)$$

where the stress boundary condition (9) has been used on the free-surface boundary Γ_f , and it is assumed that the velocity satisfies a Dirichlet condition on the remaining portion of the boundary. Application of the surface divergence theorem (see appendix A) results in

$$\int_{\Omega} (-\nabla \phi_i \cdot \boldsymbol{\sigma} + St \phi_i \mathbf{f})_{\alpha} d\Omega = - \int_{\Gamma_f} \frac{1}{Ca} (\nabla_s \phi_i)_{\alpha} d\Gamma + \int_{\gamma} \frac{1}{Ca} \phi_i m_{\alpha} d\gamma, \quad (14)$$

where γ is the contour bounding the free surface, termed the *contact line*, and \mathbf{m} is the outward unit binormal to γ , ie. \mathbf{m} is normal to γ and $\mathbf{n} \cdot \mathbf{m} = 0$ on γ . For problems in which the contact

line is kept fixed, such as those considered in the following section, this contour integral can be neglected since γ lies on the Dirichlet boundary. However, this integral must be included when considering a *dynamic* contact line.

The discretised system (14) and (12) may be written in matrix form as

$$\begin{pmatrix} \mathbf{K} & \mathbf{B} \\ \mathbf{B}^T & \mathbf{0} \end{pmatrix} \begin{pmatrix} \mathbf{u} \\ \mathbf{p} \end{pmatrix} = \begin{pmatrix} \mathbf{g} \\ 0 \end{pmatrix}, \quad (15)$$

where \mathbf{K} represents the discrete Laplacian, \mathbf{B} the discrete pressure gradient operator, and \mathbf{g} the discrete force vector including the free-surface stress boundary condition. We choose to solve this system iteratively using a preconditioned GMRES method. The preconditioning matrix \mathbf{P} is formed from an incomplete-LU factorisation of a modified form of (15) obtained by replacing the off-diagonal blocks by zero and the lower-diagonal block by a lumped pressure mass matrix \mathbf{M}_L :

$$\mathbf{P} = ILU \begin{pmatrix} \mathbf{K} & \mathbf{0} \\ \mathbf{0} & \mathbf{M}_L \end{pmatrix}. \quad (16)$$

This preconditioner is certainly not optimal (see, for example, [11] for a discussion of optimal preconditioners for Navier-Stokes and Stokes problems); however it is easy to implement and it provides significant acceleration of convergence in practice provided acceptable mesh quality is maintained. Since the Stokes problem that is solved at each time step is stationary, initial data is not required. However, in practice, the solution from the previous time step is used as an initial guess in order to minimise the number of iterations required for convergence.

3.2 Free-Surface Updates

Movement of the computational mesh is separated into two distinct phases: the normal motion of the fluid free surface, as prescribed by the computed velocity field, and; the movement of the interior mesh which is driven by mesh-quality considerations.

The kinematic boundary condition (10) is used to update the fluid free surface once the velocity field has been computed. This requires the definition of a unit normal vector at each node on the free surface. Since the finite element representation is only C^0 continuous there is no unique normal at a vertex. In fact, a separate normal can be defined at the vertex on each quadratic surface that meets at that point. It has been found, during this work, that the

commonly used mass-consistent normal [9], essentially a weighted average of the normals on the surrounding triangular surface elements, is not applicable to the three-dimensional tetrahedral Taylor-Hood finite element discretisation employed [36]. Instead an arithmetic average of the surrounding normals is used, similar in principle to that described by Cairncross *et al.* [4]. The free surface is updated with a forward Euler discretisation of (10) which removes the nonlinearity associated with the free-surface geometry. This is therefore subject to a CFL-type stability constraint on the time step that can be used.

3.3 Interior Mesh Updates

To update the interior mesh the domain is treated as a linear elastic solid subject to a prescribed displacement from the equilibrium position due to the motion of the free surface over each time step. The linear elastic problem

$$\frac{\partial}{\partial x_j} \left(C_{ijkl} \frac{\partial s_k}{\partial x_l} \right) = 0 \quad (17)$$

is solved for the unknown displacements s_k using a linear tetrahedral finite element method on a mesh consisting of the vertices of the underlying quadratic mesh. The interior vertices that lie on mesh edges are updated such that they remain at the midpoint of the vertices of that edge. The general linear elasticity tensor

$$C_{ijkl} = \lambda \delta_{ij} \delta_{kl} + \mu (\delta_{ik} \delta_{jl} + \delta_{il} \delta_{jk}) \quad (18)$$

is used here, where the coefficients λ and μ are computed from

$$\lambda = \frac{E\nu}{2(1+\nu)(1-2\nu)}, \quad \mu = \frac{E}{2(1+\nu)}. \quad (19)$$

The response of the interior mesh to the boundary motion can be altered by choosing different values for the Young's modulus E and Poisson's ratio ν . In the examples presented here, E and ν are, however, simply given the values 100 and 0.001 respectively; this choice is fairly arbitrary and appears to have little effect on the overall qualitative behaviour of the algorithm.

It is not necessary to solve the linear elasticity problem (17) exactly as the aim is simply to maintain mesh quality near the moving free surface. Hence, rather than solving directly, a Gauss-Seidel iterative approach is used. Several sweeps of the mesh vertices are performed and a local linear elasticity problem is solved at each vertex to update the node position. To

accelerate convergence of this process the interior vertices are sorted so that nodes nearest the free surface are updated first. This can be achieved by recursively ordering the vertex neighbours beginning at the fluid free surface. It is found that only two Gauss-Seidel sweeps of the mesh are required to update the interior mesh sufficiently for the examples considered below.

3.4 Discrete Remeshing

Free-surface problems involving significant change in the fluid volume (such as the droplet formation problem considered in Section 4.2 for example) cannot be effectively modelled using the mesh-movement algorithm alone. As the domain expands, the element size increases and, while the geometric quality of the elements can be maintained, the overall accuracy of the finite element method will diminish. Indeed, even in cases where the fluid volume does not change (such as the liquid-bridge problem considered in Section 4.1) the distortion of the fluid domain may be such that the mesh-movement algorithm described above cannot maintain the required mesh quality. In these cases, complete remeshing of the fluid domain is also required periodically.

There are numerous possible strategies for triggering a full remesh. In this work, a measure based upon the edge curvature κ (as in [33]) is used,

$$I_\kappa = \int_s |\kappa| ds, \quad (20)$$

which can be computed directly on the edges of the isoparametric quadratic finite element mesh. In addition, upper and lower limits are placed on the edge lengths in the mesh and a maximum number of time steps between remeshes is specified. In the examples presented here the maximum and minimum edge lengths allowed are twice and half of the initial uniform edge length respectively, and a maximum of 5000 time steps is set between adaptivity stages. The mesh generation package NETGEN [28] is used to generate a new mesh. The existing triangular surface mesh is used to define the geometry of the fluid domain, but the new mesh is not guaranteed to conform exactly to the original piecewise isoparametric quadratic surface, resulting in the possibility of a small volume change. A binary tree data structure, based upon [2], is then used to interpolate efficiently solution data from the original mesh to the nodes in the adapted mesh. For Stokes flow, the interpolated solution is used as an initial guess for

the iterative solution at the next time step, whilst for Navier-Stokes flows it is required for the initial state at the next time step. The computational cost of the discrete remeshing process is small compared to the flow solution, since typically many hundreds of time steps are taken between remeshing stages.

4 COMPUTATIONAL EXAMPLES

In this section two representative test problems are solved using the algorithm described above. In the first of these the total fluid volume remains constant, whilst in the second the volume grows with time due to an inflow boundary.

4.1 Liquid Bridge

The liquid-bridge problems considered here comprise an initially cylindrical fluid domain pinned at static circular contact lines to two parallel vertical walls. The walls move with an equal and opposite velocity, stretching the free surface, which must adjust such that the fluid volume is conserved. The initial domain, a fluid cylinder of radius 1 and length 1, is discretised with 3406 nodes and 2054 isoparametric quadratic tetrahedral elements. The initial mesh is generated with a target uniform edge length of 0.1 and a constant time step of 0.001 is used. In the absence of gravity ($St = 0$) the fluid domain evolves in an axisymmetric manner. Figure 1 illustrates the free-surface shape at four instants during the simulation. In the second example a gravitational force is introduced ($St = 1$) acting perpendicular to the initial axis of symmetry of the fluid. The capillary number $Ca = 1$ in both examples. Figure 2 illustrates the free-surface shape at the same four instants during this simulation. Due to the motion of the solid boundaries, the edge length on the free surface neighbouring the walls is increased relatively quickly, which necessitates regular discrete remeshing of the domain. This is because the kinematic boundary condition (10) constrains the nodes on the free surface to move in only the direction normal to it and hence the mesh becomes distorted near the solid walls, which are moving almost tangentially to the free surface in the early stages of the simulation. The examples shown have been remeshed twelve times during the simulation. Since the volume remains theoretically constant during the simulation the number of degrees of freedom remains approximately constant despite the remeshing steps. In practice

there is a small volume change, due to both the discrete nature of the computational algorithm employed and the occasional remeshing of the entire domain. In the two examples considered, the volume change is approximately 0.5% of the initial volume over the entire simulation. However, almost all of the observed error is introduced at the discrete remeshing stages, which introduces a volume change which is an order of magnitude greater than that due to the explicit update of the free surface.

4.2 Droplet Formation

The droplet-formation problem comprises a vertically aligned cylindrical tube of radius 1 with fluid fed into the top through a uniform parabolic velocity field. At the bottom the initially hemispherical free surface of the fluid grows to accommodate the increase in fluid volume. Hence, physically, the problem is a model of a slowly-forming drip on a leaking tap. The contact line, where the fluid free-surface meets the opening of the tube, is fixed and treated as static. For this example, the zero-gravity case is not particularly interesting since the droplet will just develop, under the equilibrating action of surface tension, as an expanding sphere attached to the cylindrical tube. Hence we only provide results where gravity is present, acting in the axial direction of the tube. The initial mesh is generated with a target uniform edge length of 0.1 and a constant time step of 0.001 is used. Figure 3 illustrates the free surface shape at three instants during a simulation in which the Stokes number $St = 2$ and Capillary number $Ca = 1$. As the domain expands the mesh movement algorithm redistributes the internal nodes to allow for the boundary motion. Thus the mesh size necessarily grows, requiring remeshing of the fluid domain, giving a corresponding increase in the discrete problem size as time evolves. In the case shown in Figure 3(a) there are initially 2514 nodes and 1430 elements while after six remeshing stages (Figure 3(c)) there are 4938 nodes and 2639 elements. This has implications for the cost of the iterative solution at each time step. If an optimal preconditioner were used the number of iterations would remain fixed but the cost per iteration would grow. However, since our simpler preconditioner is not optimal the number of iterations, as well as the cost per iteration, grows with the problem size. This issue of deteriorating convergence rate still needs to be addressed in order to simulate the formation of the droplet right up to the point immediately prior to break-off.

5 DISCUSSION AND FURTHER WORK

In this paper we have introduced an adaptive algorithm for the solution of three-dimensional moving-boundary problems based primarily upon the use of mesh movement but also exploiting discrete remeshing when necessary. Previous work in this area has been typically based upon linear tetrahedral or hexahedral finite element approximations, however here the governing equations are discretised with an *a priori* stable tetrahedral Taylor-Hood finite element method. This method requires no additional artificial stabilisation and includes an isoparametric quadratic approximation of the problem geometry allowing a more accurate model of the evolving free surface and of the surface tension forces acting on it. Application of this algorithm to two fully three-dimensional problems has been described in order to demonstrate the significant potential of the approach. At this stage, however, further development is still required in order to ensure that this potentially powerful approach can be made sufficiently robust to be applied to the widest possible range of free-surface flow problems.

At present the free surface is updated by allowing normal motion in order to satisfy the kinematic boundary condition (10). It would be advantageous to allow free-surface nodes to move in tangential directions as well since this is likely to reduce the frequency of the discrete remeshing stages that is required. In the early stages of the liquid-bridge problem considered in Section 4.1, the end planes are moving almost tangentially to the free surface and so stretching occurs in the elements near to these planes: this could be avoided if suitable tangential motion of the free-surface nodes was allowed.

Discrete remeshing is vital if long-time simulations of evolving fluid surfaces are to be achieved. The simple rules described in Section 3.4 for driving the remeshing process can be enhanced in a number of ways, to include for example other measures of surface mesh quality, and further investigation is required to produce a precise strategy. In addition to the computational cost associated with the discrete remeshing stage, our current implementation (based up on the use of the NETGEN software tool [28]) also causes a small, but not negligible, change in the volume of the fluid. It is necessary therefore to investigate the most effective way of eliminating this volume change from the remeshing procedure. Numerous approaches are possible, however it is important to ensure that local accuracy in the geometry representation is maintained as well as global volume conservation.

As mentioned in Section 4, the computational cost of solving the problem iteratively in-

creases with the problem size. Optimal preconditioners for Stokes and Navier-Stokes problems have been presented by [11], which bound the number of iterations required independently of the mesh size, based on an optimal *inner* solve of the discrete Laplace equation using a multigrid method. For the unstructured tetrahedral grids employed here, this approach is not directly applicable, since the required hierarchy of grids is not available. However, recent work [22] has suggested the use of algebraic multigrid techniques for this component of the method.

The examples provided in this paper show the performance of the algorithm on problems for which the contact line is fixed. In addition to problems of this type, those in which the contact line moves, containing a so-called *dynamic contact line*, are of significant practical interest. Examples include the spreading of a droplet across a surface or the capillary rise of a fluid in a narrow tube. This is an extension of the work we are currently undertaking, initially through the approach presented in [1].

Acknowledgements

The authors wish to thank the EPSRC for funding this work through grant GR/R25453/01.

A THE SURFACE DIVERGENCE THEOREM

In the notation of Subsection 3.1 the surface divergence theorem, [37], states that

$$\int_{\Gamma_f} \nabla_s \cdot \mathbf{v} \, d\Gamma = \int_{\gamma} \mathbf{v} \cdot \mathbf{m} \, d\gamma - \int_{\Gamma_f} 2H (\mathbf{v} \cdot \mathbf{n}) \, d\Gamma, \quad (21)$$

where $H = -\frac{1}{2} \nabla_s \cdot \mathbf{n}$ is the surface mean curvature. Hence, application of (21) with $\mathbf{v} = \frac{1}{Ca} \phi_i \mathbf{e}_\alpha$ (where \mathbf{e}_α is the unit vector in coordinate direction α) gives:

$$\int_{\Gamma_f} \nabla_s \cdot \left(\frac{1}{Ca} \phi_i \mathbf{e}_\alpha \right) \, d\Gamma = \int_{\gamma} \left(\frac{1}{Ca} \phi_i \mathbf{e}_\alpha \right) \cdot \mathbf{m} \, d\gamma + \int_{\Gamma_f} (\nabla_s \cdot \mathbf{n}) \left(\frac{1}{Ca} \phi_i \mathbf{e}_\alpha \right) \cdot \mathbf{n} \, d\Gamma. \quad (22)$$

Hence

$$- \int_{\Gamma_f} \phi_i \frac{1}{Ca} (\nabla_s \cdot \mathbf{n}) \mathbf{n} \cdot \mathbf{e}_\alpha \, d\Gamma = - \int_{\Gamma_f} \frac{1}{Ca} \nabla_s \cdot (\phi_i \mathbf{e}_\alpha) \, d\Gamma + \int_{\gamma} \frac{1}{Ca} \phi_i \mathbf{m} \cdot \mathbf{e}_\alpha \, d\gamma \quad (23)$$

$$= - \int_{\Gamma_f} \frac{1}{Ca} \nabla_s \phi_i \cdot \mathbf{e}_\alpha \, d\Gamma + \int_{\gamma} \frac{1}{Ca} \phi_i \mathbf{m} \cdot \mathbf{e}_\alpha \, d\gamma. \quad (24)$$

This last expression demonstrates the equivalence of (13) and (14) as claimed.

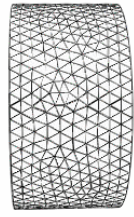
References

- [1] Baer, T.A., Cairncross, R.A., Schunk, P.R., Rao, R.R., and Sackinger, P.A. (2000). A finite element method for free surface flows of incompressible fluids in three dimensions. Part II. Dynamic wetting lines. *Int. J. Num. Meth. Fluids.* **33**, 405-427.
- [2] Bonet, J. and Peraire, J. (1991). An alternating digital tree (ADT) algorithm for 3d geometric searching and intersection problems. *Int. J. Num. Meth. Engg.* **31**, 1-17.
- [3] Bunner, B. and Tryggvason, G. (1999). Direct numerical simulation of three-dimensional bubbly flows. *Phys. of Fluids (Letters)*. **11**, 1967-1969.
- [4] Cairncross, R.A., Schunk, P.R., Baer, T.A., Rao, R.R., and Sackinger, P.A. (2000). A finite element method for free surface flows of incompressible fluids in three dimensions. Part I. Boundary fitted mesh motion. *Int. J. Num. Meth. Fluids.* **33**, 375-403.
- [5] Cerne, G., Petelin, S. and Tiselj, I. (2002). Numerical errors of the volume-of-fluid interface tracking algorithm. *Int. J. Num. Meth. Fluids.* **38**, 329-350.
- [6] Gaskell, P.H., Jimack, P.K., Sellier M. and Thompson, H.M. (2004). Efficient and accurate time adaptive multigrid simulations of droplet spreading. *Int. J. Num. Meth. Fluids.* (To appear).
- [7] Gaskell, P.H., Jimack, P.K., Sellier M., Thompson, H.M. and Wilson, M.C.T. (2004). Gravity-driven flow of continuous thin liquid films on non-porous substrates with topography. *J. Fluid Mech.* (To appear).
- [8] Gaskell, P.H., Savage, M.D., Summers J.L. and Thompson, H.M. (1995). Modelling and analysis of meniscus roll coating. *J. Fluid Mech.* **298**, 113-137.
- [9] Gresho, P.M., and Sani, R.L. (2000). *Incompressible Flow and the Finite Element Method. Volume 2: Isothermal Laminar Flow.* Wiley.
- [10] Hirt, C.W. and Nichols, B.D. (1981). Volume of fluids methods for the dynamics of free boundaries. *J. Comput. Phys.* **39**, 201-225.
- [11] Kay, D., Loghin, D. and Wathen, A.J. (2001). A preconditioner for the steady-state Navier-Stokes equations. *SIAM J. Sci. Comput.* **24**, 237-256.

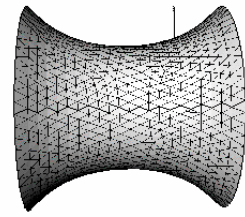
- [12] Kuiken, H.K. (1990). Viscous sintering: the surface-tension-driven flow of a liquid form under the influence of curvature gradients at its surface. *J. Fluid Mech.* **214**, 503-515.
- [13] Lynch, D.R. and O'Neill, K. (1981). Continuously deforming finite elements for the solution of parabolic problems, with and without phase change. *Int. J. Num. Meth. Fluids.* **17**, 81-96.
- [14] Marar, O.K. and Troians, S.M. (1999). The development of transient fingering patterns during the spreading of surfactant coated films. *Phys. of Fluids.* **11**, 3232-3246.
- [15] Mashayek, F. and Ashgriz, N. (1995). A spine-flux method for simulating free surface flows. *J. Comput. Phys.* **122**, 367-399.
- [16] Miyata, H. (1986). Finite difference simulation of breaking waves. *J. Comput. Phys.* **65**, 179-214.
- [17] Moriarty, J.A., Schwartz, L.W. and Tuck, E.O. (1991). Unsteady spreading of thin liquid films with small surface tension. *Phys. of Fluids.* **3**, 733-751.
- [18] Muttin, F., Coupez, T., Bellet M. and Chenot, J.L. (1993). Lagrangian finite-element analysis of time-dependent free-surface flow using an automatic remeshing technique – application to metal casting. *Int. J. Num. Meth. Engg.* **36**, 2001-2015.
- [19] Osher, S. and Sethian, J.A. (1988). Fronts propagating with curvature-dependent speed: algorithms based on Hamilton-Jacobi formulations. *J. Comput. Phys.* **79**, 1-49.
- [20] Peterson, R.C., Jimack, P.K., and Kelmanson, M.A. (1999). The solution of two-dimensional free-surface problems using automatic mesh generation. *Int. J. Num. Meth. Fluids.* **31**, 937-960.
- [21] Peterson, R.C., Jimack, P.K., and Kelmanson, M.A. (2001). On the stability of viscous, free-surface flow supported by a rotating cylinder. *Proc. Roy. Soc. Lond.* **A457**, 1427-1445.
- [22] Powell, C.E. and Silvester, D.J. (2002). Black-box preconditioning for mixed formulation of self-adjoint elliptic PDEs. *Numerical Analysis Report No. 415*. Dept. of Mathematics, Univ. of Manchester.

- [23] Pozrikidis, C. and Thoroddsen, S.T. (1991). The deformation of a liquid film flowing down an inclined plane wall over a small particle arrested on the wall. *Phil. Trans. Roy. Soc.* **A340**, 1-45.
- [24] Ramaswamy, B. and Kawahara, M. (1987). Lagrangian finite-element analysis applied to viscous free-surface fluid flow. *Int. J. Num. Meth. Fluids.* **7**, 953-984.
- [25] Saito, H. and Scriven, L.E. (1981). Study of coating flow by the finite element method. *J. Comput. Phys.* **42**, 53-76.
- [26] Scardovelli, R. and Zaleski, S. (1999). Direct numerical simulation of free-surface and interfacial flow. *Annual Rev. Fluid Mech.* **31**, 567-603.
- [27] Schmidt, A. (1996). Computation of three dimensional dendrites with finite elements. *J. Comput. Phys.* **125**, 293-312.
- [28] Schöberl, J. (1997). NETGEN - An advancing front 2D/3D-mesh generator based on abstract rules. *Comput. Visual. Sci.* **1**, 41-52.
- [29] Schwartz, L.W. and Eley, R.R. (1998). Simulation of droplet motion on low-energy and heterogeneous surfaces. *J. Colloid Inter. Sci.* **202**, 173-188.
- [30] Sethian, J.A. (1996). *Level Set Methods: Evolving Interfaces in Geometry, Fluid Mechanics, Computer Vision and Material Sciences*. Cambridge University Press: Cambridge, UK.
- [31] Soulaïmani, A. and Saad, Y. (1998). An arbitrary Lagrangian-Eulerian finite element method for solving three-dimensional free surface flows. *Comput. Meth. Appl. Mech. Engrg.* **162**, 70-106.
- [32] Stone, H.A. (1994). Dynamics of drop deformation and breakup in viscous fluids. *Annual Rev. Fluid Mech.* **26**, 65-102.
- [33] Struik, D.J. (1961). *Differential Geometry (second edition)*. Adison-Wesley.
- [34] Tomé, M.F., Filho, A.C., Cuminato, J.A., Mangiavacchi, N. and McKee, S. (2001). GENSMAC3D: a numerical method for solving unsteady three-dimensional free surface flows. *Int. J. Num. Meth. Fluids.* **37**, 747-796.

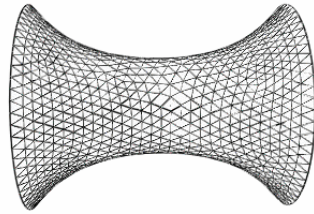
- [35] van der Vorst, G.A.L. and Mattheij, R.M.M. and Kuiken, H.K. (1992). A boundary element method for two-dimensional viscous sintering. *J. of Comput. Phys.* **100**, 50-63.
- [36] Walkley, M.A., Gaskell, P.H., Jimack, P.K., Kelmanson, M.A., Summers, J.L., and Wilson, M.C.T. (2004). On the calculation of normals in free-surface flow problems. *Comm. Num. Meth. Engrg.* (To appear).
- [37] Weatherburn, C.E. (1939). *Differential Geometry of Three Dimensions*. Cambridge University Press.
- [38] Zhou, H., and Derby, J.J. (2001). An assessment of a parallel, finite element method for three-dimensional, moving-boundary flows driven by capillarity for simulation of viscous sintering. *Int. J. Num. Meth. Fluids*. **36**, 841-865.



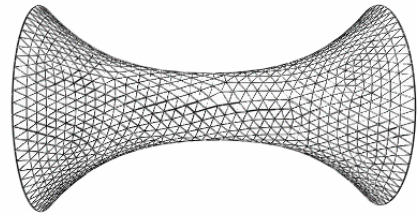
(a) Time 0.0



(b) Time 0.8

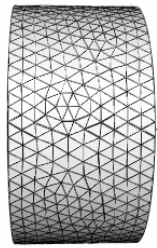


(c) Time 1.6

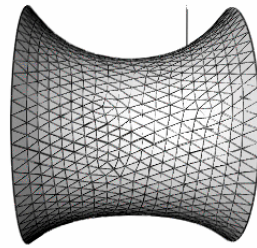


(d) Time 2.4

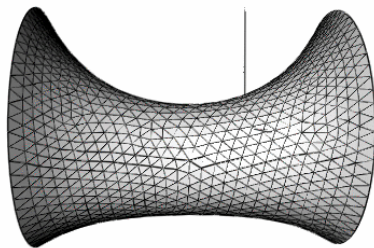
Figure 1: Liquid-bridge problem: $St = 0$, $Ca = 1$



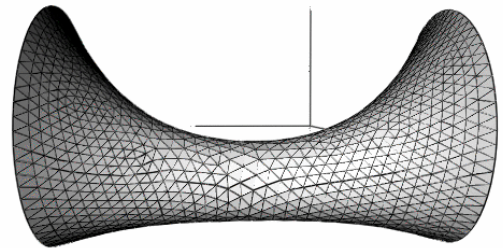
(a) Time 0.0



(b) Time 0.8

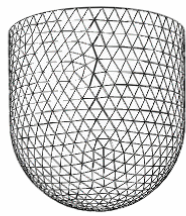


(c) Time 1.6

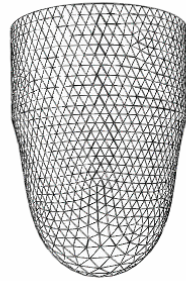


(d) Time 2.4

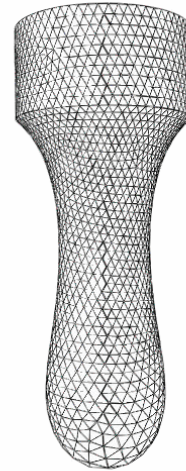
Figure 2: Liquid-bridge problem: $St = 1, Ca = 1$



(a) Time 0.0



(b) Time 2.8



(c) Time 5.6

Figure 3: Droplet-formation problem: $St = 2$, $Ca = 1$